



# Effect of Ag-decorated MWCNT on the mechanical and thermal property of Sn58Bi solder joints for FCLED package

Choong-Jae Lee<sup>1</sup> · Woo-Ram Myung<sup>2</sup> · Bum-Geun Park<sup>3</sup> · Seung-Boo Jung<sup>1</sup>

Received: 14 March 2020 / Revised: 3 May 2020 / Accepted: 6 May 2020 / Published online: 13 May 2020  
© Springer Science+Business Media, LLC, part of Springer Nature 2020

## Abstract

Ag-decorated multi-walled carbon nanotubes (Ag-MWCNT) were investigated for use in Sn58Bi solder joints for FCLED packages. Among lead-free solders, Sn58Bi solder has been identified as a candidate for widespread use because of its low melting temperature and high tensile strength. However, Sn58Bi solder is brittle, and it is difficult to relieve it from an impact shock. To overcome these limitations, the bonding characteristics of Sn58Bi solder have been improved with Ag-MWCNT. Ag-MWCNT composite solder paste is fabricated by mixing Ag-MWCNTs of various concentrations with solder paste, and the FCLED chips are bonded on the printed circuit board. The thermal, electrical, and mechanical properties of the solder joints are investigated using various tests. The bonding strength of the Sn58Bi solder with the Ag-MWCNTs increased by 16% compared to that without it. Furthermore, the thermal resistance of the solder alloy decreased by a factor of 2 with the addition of 0.1 wt% Ag-MWCNT.

## 1 Introduction

The trend in electronics packaging is for solder joints to become smaller and smaller in size as electronic components are further miniaturized. Solder joints provide an interconnection between the chip and the substrate, and they play various important roles at different levels of the electronics assembly, which demands improvements in their thermo-mechanical and electrical properties [1, 2].

The Sn58Bi alloy has an eutectic composition and is an attractive lead-free substitute since it can be used at a low temperature [3]. Low-temperature soldering is necessary to prevent thermal damage of electronic devices during reflow [4]. Low-temperature soldering can reduce warpage, which is induced by a mismatch of coefficients of thermal expansion (CTE) between different materials during

high-temperature processing [5]. In addition, it is also possible to reduce damage by decreasing the peak temperature and the time for the reflow, which creates economic advantages during manufacturing [6].

Sn58Bi solder offers improved mechanical properties, such as yield strength, shear strength, and creep resistance, when compared to Sn37%Pb solder [7–10]. However, the ductility of Sn58Bi is lower than that of Sn–Pb solder due to the brittleness of Bi, which leads to critical problems in the mechanical reliability of the solder joints [11]. Many researchers have studied alternative methods to improve the mechanical properties of the Sn58Bi solder. One solution is to add other elements in the Sn–Bi alloy.

Previous research has shown that Ag can improve the ductility of the Sn58Bi solder through microstructural refinement of the Sn58Bi solder alloy, which improves the mechanical properties of the solder joints [12–15]. Another method to improve the mechanical properties of the solder joints is the addition of epoxy in the Sn–Bi solder paste. An epoxy fillet is formed around the solder joint during reflow, and the shear strength and drop reliability of the epoxy-containing Sn58Bi are higher than those of the Sn58Bi solder [16–18]. Another approach is to add carbon nanotubes to reinforce the mechanical properties of the solder.

With the addition of the CNTs, the tensile strength and the elongation of the Sn–Bi solder improved, and the thickness of the intermetallic compound (IMC) decreased

✉ Seung-Boo Jung  
sbjung@skku.edu

<sup>1</sup> School of Advanced Materials Science & Engineering, Sungkyunkwan University, 2066 Seobu-ro, Jangan-gu, Suwon 16419, Republic of Korea

<sup>2</sup> Test & System Package, SAMSUNG Electronics, 158 Baebang-ro, Baebang-eup, Asan-si 32489, Republic of Korea

<sup>3</sup> Visual Display Business, SAMSUNG Electronics, 129 Samsung-ro, Yeongtong-gu, Suwon-si 16677, Republic of Korea

[18–20]. CNTs exhibit the highest elastic modulus on the order of 1–3 TPa [21] and also have superior electrical and thermal properties [22]. However, CNTs have a low density, resulting in a big difference in density and weak bonding characteristics with the solder matrix that lead to severe segregation and non-uniform dispersion during reflow [20, 23, 24]. Ag-decorated MWCNTs (Ag-MWCNTs) are proposed to solve these segregation problems. The Ag atoms can form a continuous coating on the MWCNTs with a significant binding energy [25], and the Ag-MWCNTs are embedded well in the solder matrix after soldering [26].

We investigated the thermal, mechanical, and electrical properties of the Sn58Bi solder with added Ag-MWCNTs for use as solder joints in FCLED packages by measuring the thermal conductivity, bonding reliability, and electrical resistance of the solder joints.

## 2 Experimental procedure

The Ag-MWCNT composite materials were synthesized by applying a functionalizing and reducing process. Commercial MWCNTs have diameters of about 10–20 nm and length of 15  $\mu\text{m}$ . To get rid of the carbon impurities and improve the efficiency of the acid treatment, the MWCNTs were annealed at 600  $^{\circ}\text{C}$ . Then, the MWCNTs were functionalized through an acid treatment with a mixture of  $\text{H}_2\text{SO}_4$  and  $\text{HNO}_3$  to form carboxyl groups ( $-\text{COOH}$ ) onto the MWCNTs. After acid treatment, the functionalized MWCNTs were washed using DI water.  $\text{CH}_3\text{COOAg}$  was then added to the MWCNT colloids and was reacted by stirring and sonicating. Next, the colloidal solution was stirred at 100  $^{\circ}\text{C}$ , and calcination was performed at 300  $^{\circ}\text{C}$ . The synthesized Ag-MWCNTs nanocomposites were investigated via high-resolution transmission electron microscopy (HRTEM, JEM ARM 200F, JOEL, Ltd., Japan) to confirm the presence of the Ag nanoparticles on the MWCNTs, as shown in Fig. 1.

A commercial GaN-type FCLED chip was used to evaluate the thermal, electrical, and mechanical properties of the Ag-MWCNT composite solder. We fabricated the substrate with an Al metal PCB with an OSP surface-finished Cu electrode, which had a circular opening with diameter of 230  $\mu\text{m}$ . The FCLED chips and metal PCB were bonded via thermal compression using Sn58Bi solder paste with various Ag-MWCNTs concentrations (0, 0.05, 0.1, and 0.3 wt%) using a flip-chip bonder for 30 s with a maximum temperature of 190  $^{\circ}\text{C}$ .

Raman spectra were recorded in the backscattering geometry on a Micro-Raman spectrometer (Alpha300M+, WITec, Germany) in conjunction with a confocal microscope using argon laser excitation (532 nm and 50 mW) to obtain the distribution of Ag-MWCNT in the solder matrix. The incident laser beam was focused onto the specimen surface forming a laser spot of about 3  $\mu\text{m}$  in diameter.

A die shear test was performed using a bond tester (PTR-1000, Rhesca Co., Japan). The shear height and shear speed were fixed at 50  $\mu\text{m}$  and 200  $\mu\text{m/s}$ , respectively. The cross-sectional microstructures and fracture surface of solder joints after the shear test were investigated using a scanning electron microscope (SEM, Hitachi, S-3000H, Japan). The chemical composition of the intermetallic compounds (IMC) layer was determined using an energy dispersive spectrometer (EDS, Horiba, EMAX-7021-H, England). Furthermore, an elementary mapping of the IMC layers was conducted with an electron probe micro-analyzer (EPMA, JEOL, JXA-8500F, Japan). The electrical properties of the FCLED packages were evaluated by measuring the I–V curves with a semiconductor parameter analyzer (HP4145B, Agilent Technologies, USA). Direct currents were applied on solder joints, with a range of electrical potentials from 0 to 3 V.

The thermal conductivities of the Sn58Bi solders containing various concentrations of Ag-MWCNTs (0, 0.05, 0.1, and 0.3 wt%) were investigated with the hot disk method. The insulated Kapton sensor in a thermal constant analyzer (TPS 2500S, Hot Disk, Sweden) was sandwiched between

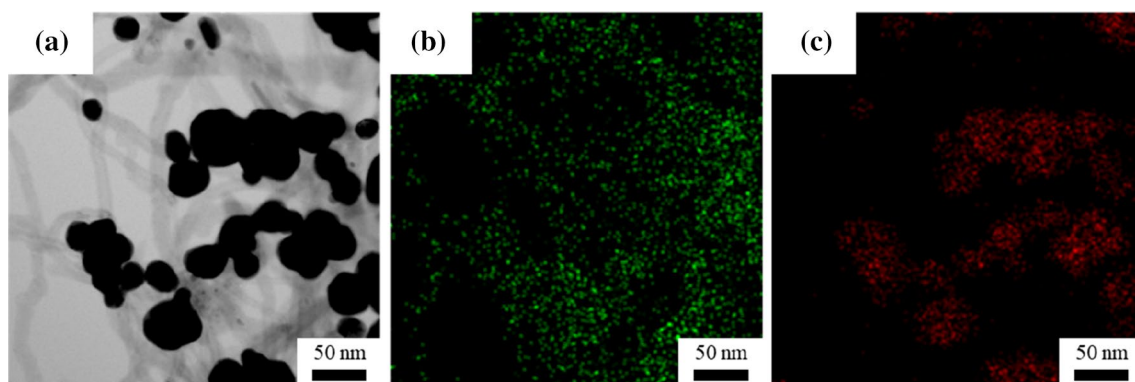


**Fig. 1** a HRTEM micrographs of the Ag-MWCNTs and EDS analysis of b carbon and c Ag

two Sn58Bi solder disks containing Ag-MWCNTs. The used solder disks had a diameter of 50 mm with a thickness of 200  $\mu\text{m}$ .

The temperature profiles of each FCLED package and substrate were measured with an infrared (IR) camera (FLIR T425, FLIR Co. Ltd., Sweden) and a thermocouple (GL220, GRAPHTEC Co. Ltd., Japan) when operating with a current of 450 mA. The thermal resistance of the Ag-MWCNT composite solders was also measured under a current of 450 mA to evaluate the thermal properties of the FCLED packages using a T3ster thermal transient tester (T3ster 2000/100, MicReD Co. Ltd., USA).

### 3 Results and discussion

Figure 2 shows SEM micrographs of the Sn58Bi solder joints with various Ag-MWCNT contents after reflow. The microstructures of the Sn58Bi solder show a lamellar structure that consists of a Bi-rich and Sn-rich phase in the solder matrix. In the substrate side,  $\text{Cu}_6\text{Sn}_5$  IMC, which had a scalloped morphology, formed by a reaction between the Cu pad and Sn in the solder. The Cu–Bi binary phase diagram [27] shows that no intermetallic phase between Bi and Cu exists. Cu and Bi are essentially mutually insoluble under 270  $^\circ\text{C}$  [28]. In the FCLED chip side, the interfacial IMC layer consisted of  $(\text{Ni,Cu})_3\text{Sn}_4$ . A thick scallop layer of Cu–Ni–Sn was observed at the interface in the Sn58Bi solder joints. However, a planar Cu–Ni–Sn layer was observed at Sn58Bi joints with Ag-MWCNTs, as shown in Fig. 2b–d. The thickness of the IMC layer for the Sn58Bi solder joints in the

FCLED chip side was 0.72  $\mu\text{m}$ , while for the Sn–Bi/0.05Ag-MWCNT, Sn–Bi/0.1Ag-MWCNT, Sn–Bi/0.3Ag-MWCNT joints, and the thicknesses were 0.52  $\mu\text{m}$ , 0.5  $\mu\text{m}$ , and 0.43  $\mu\text{m}$ , respectively. The IMC thickness of the solder joints decreased with the Ag-MWCNTs. The Ag-MWCNTs in the solder matrix seemed to restrain the diffusion of Sn atoms towards the interface of the Ni layer and Cu pad, as shown in Fig. 3. Thus, the presence of the Ag-MWCNTs as reinforcements in the solder joints can effectively slow down the growth of the IMC layers.

Figure 4 shows the elemental mapping of the Sn58Bi solder and Sn58Bi/0.3Ag-MWCNT joints as reflowed. The results indicate that the Cu–Sn IMC particles in the solder matrix and rod-shaped IMC formed at the interface of chip side, as shown Fig. 4a. In the case of the

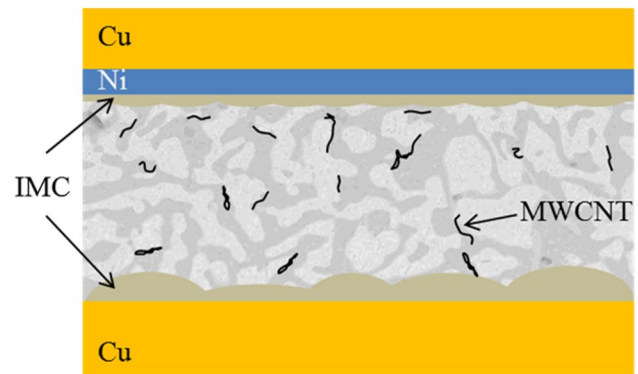


**Fig. 3** Schematic diagram showing the presence of Ag-MWCNTs in the composite solder matrix

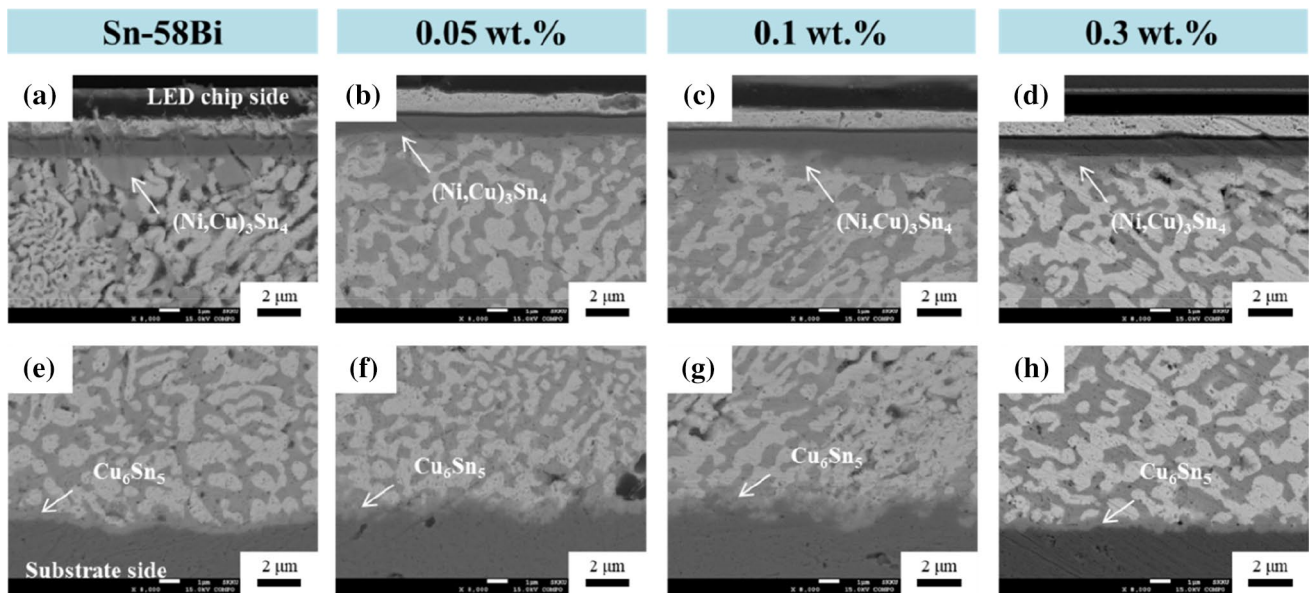


**Fig. 2** Cross-sectional SEM micrographs of the solder joints with the addition of Ag-MWCNTs; **a–d** chip side and **e–h** substrate side

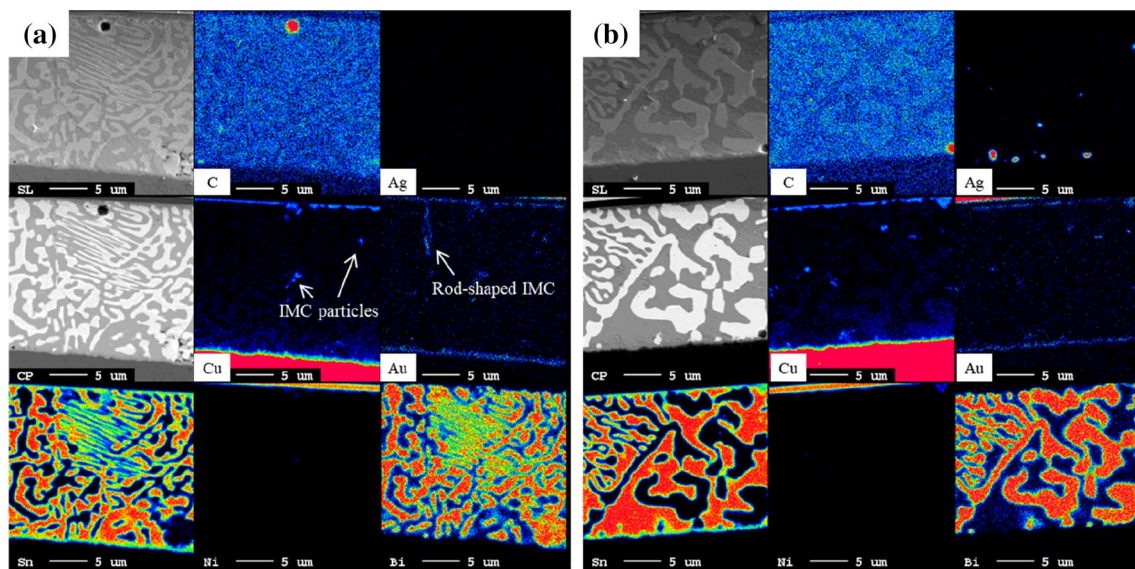


**Fig. 4** EPMA analysis of the solder joints; **a** Sn58Bi, **b** Sn58Bi with 0.3 wt% Ag-MWCNTs

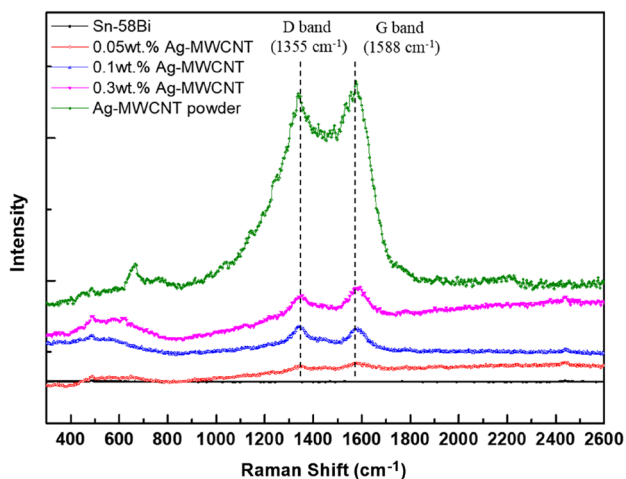


**Fig. 5** Raman spectra of the Sn58Bi solder with Ag-MWCNTs

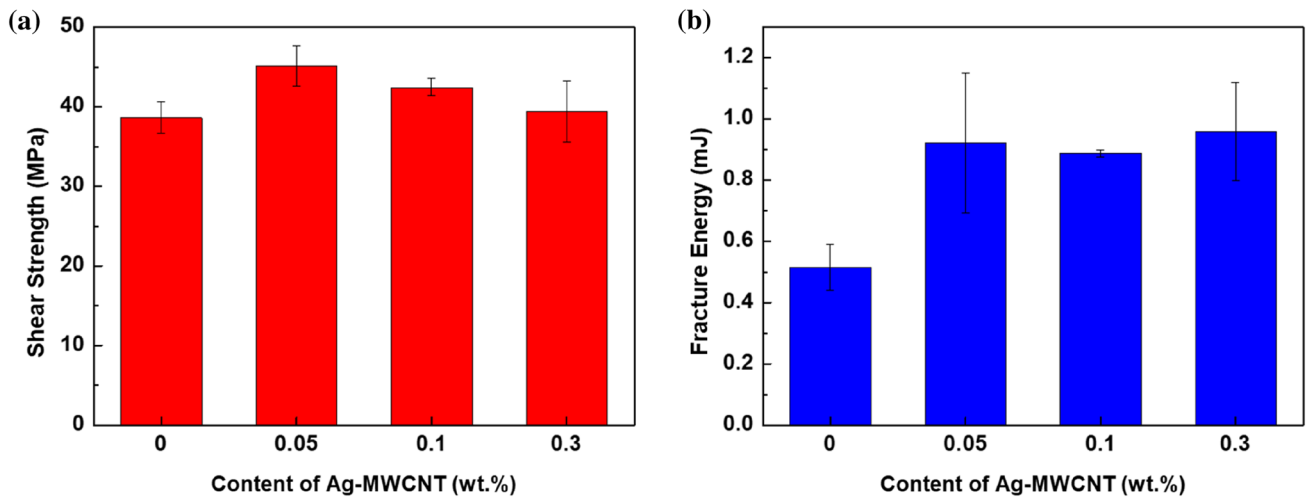
Sn58Bi/0.3Ag-MWCNT joint, the Ag particles were identified, and a rod-shaped IMC was not identified in the solder matrix, as shown in Fig. 4b. This means that the Ag-decorated MWCNTs were dispersed in the solder matrix and prevent the IMC layer growth.

Figure 5 shows the Raman spectra of the Ag-MWCNT powder and Sn58Bi solder with various Ag-MWCNT contents. The two main typical graphite bands are present in the Raman spectrum of the MWCNTs: the bands at  $1580\text{ cm}^{-1}$  (G band) assigned to the in-plane vibration of the C–C bond (G band) with a shoulder around  $1604\text{ cm}^{-1}$ , typical of defective graphite-like materials and the band at  $1355\text{ cm}^{-1}$  (D band) activated by the presence of disorder in the carbon system [29, 30]. These peaks of the MWCNT were

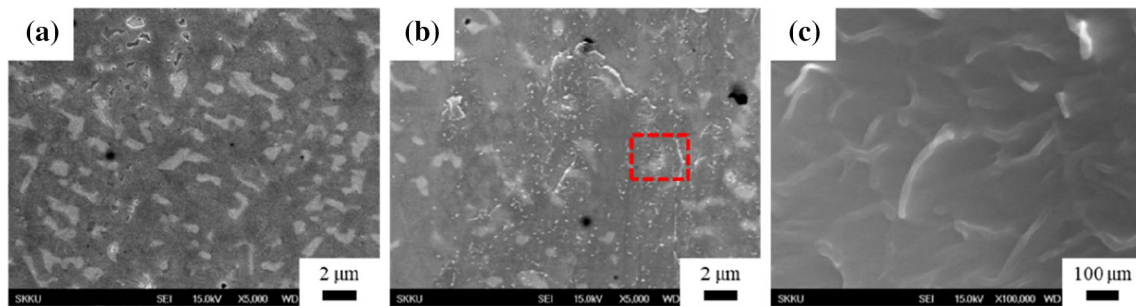
observed with the Sn58Bi solder matrix with 0.05, 0.1, and 0.3Ag-MWCNTs. This means that the Ag-MWCNTs were homogeneously dispersed in the solder matrix.

Figure 6 shows the shear strength and the fracture energy of the solder joints after the shear test. The shear strength of the Sn58Bi solder joints with the addition of Ag-MWCNTs was higher than that of the pure Sn58Bi solder joints. The relative improvement was observed to be the most significant with the addition of 0.05 wt% of Ag-MWCNTs, for which the shear strength values increased by 16% compared to pure Sn58Bi solder joints. The mechanical properties of the Sn58Bi solders improved through various strengthening mechanisms due to MWCNTs. First, the thinner IMC layer of the solder joints could be the reason since the MWCNTs disturbed the atomic diffusion, and then the dispersed Ag-MWCNTs in the solder joints could have distributed the load to the solder alloys. Finally, the superior tensile strength of the Ag-MWCNTs could improve the Sn58Bi solders [1, 31].

However, the average shear strength of the solder joint exhibited a decrease with contents higher than 0.05 wt% Ag-MWCNTs. It was thought that small clusters formed due to the strong van der Waals forces among the MWCNTs, which result in an interruption of the effective bonding at the interfaces between the solder and bonding pads [1, 32]. The fracture energy of the Sn58Bi solder with Ag-MWCNTs was higher than that of the Sn58Bi solder joint, with similar values with the addition of Ag-MWCNTs regardless of the Ag-MWCNTs content. Figure 7 shows the fracture surfaces of the solder joints after the shear test. The fracture of all samples occurred at the chip side. Smoothly fractured surfaces were observed in most solders, as shown in Fig. 7a. Also, partially dispersed



**Fig. 6** **a** Shear strength and **b** fracture energy of the solder joints depending on the contents of Ag-MWCNTs



**Fig. 7** Fracture surfaces of the solder joint after the shear test; **a** Sn58Bi, **b** Sn58Bi with 0.3 wt% Ag-MWCNTs, **c** magnified view of **b**

Ag-MWCNTs were observed on the fractured surface of the samples with the addition of Ag-MWCNTs, as shown in Fig. 7b–c. This could be evidence that the dispersed Ag-MWCNTs lead to an increase in the fracture energy and therefore, an improvement in the mechanical properties of the solder joints.

The electrical resistance of the solder with various Ag-MWCNT contents was analyzed by calculating the slope of the  $I$ – $V$  curve. Figure 8 shows the  $I$ – $V$  curve of the Ag-MWCNT composite solders. We evaluate the electrical resistance of the FCLED packages by operating the FCLED packages at various voltages. The resistance was calculated by measuring the current simultaneously while controlling voltages during the FCLED package operation. The electrical resistance of the Sn58Bi solders decreased about 6% for the 0.05 wt% Ag-MWCNT composite because of the net structure of the composite and thinner IMC layer than Sn58Bi solders as shown in the results of the microstructure. The Ag-MWCNTs in the solder matrix could function as an electrical path.

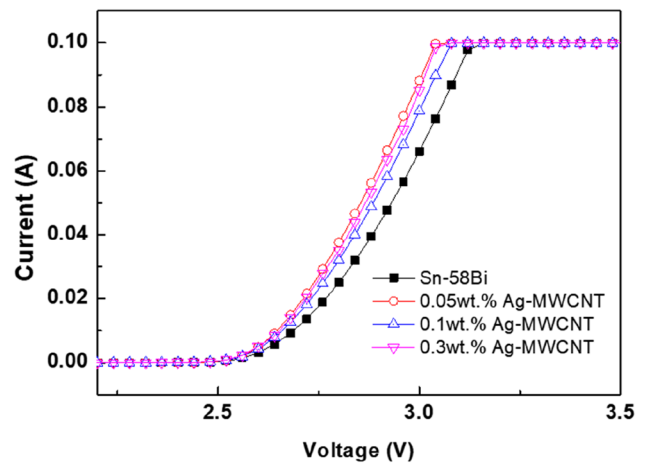


**Fig. 8**  $I$ – $V$  curve of the FCLED packages as function of the addition of Ag-MWCNTs

Generally, the formation of precipitates in a pure metal degrades the electrical properties [33]. However, previous research has demonstrated that  $\text{Ag}_3\text{Sn}$  in the solder matrix

does not have a significant effect on the electrical conductivity [34]. Therefore, the electrical resistivity of the solder joint increased due to IMC growth at the solder joints.

The thermal conductivity of the Sn58Bi solder also improved with the Ag-MWCNT composites. The thermal conductivity of the Sn58Bi solders improved about 8% with the Ag-MWCNTs in the solder matrix. Figure 9 shows the thermal conductivity of the pure Sn58Bi and that with 0.05, 0.1, and 0.3 wt% of Ag-MWCNTs. The thermal conductivity of the Sn58Bi solder with Ag-MWCNTs was higher than that of the pure Sn58Bi solder. Thermal conductivities of 20.32 and 23.17 W/mK were achieved with the pure Sn58Bi solder and the Sn58Bi/0.1Ag-MWCNT, respectively. The thermal conductivity improved by 8%. The Ag-MWCNTs embedded in the Sn58Bi solder formed thermally

conductive networks, resulting in an increase in the thermal conductivity.

Figure 10 shows the variation in temperature of the FCLED packages and the thermal resistance profiles of the solder joints with Ag-MWCNTs under a constant operating current. The operating temperature and thermal resistance of the FCLED packages show similar results. The FCLED package with Sn58Bi/0.1Ag-MWCNT solder joints exhibited the lowest temperature, as shown in Fig. 10a. The chip surface temperature could decrease by about 5 °C when compared to the Sn58Bi solder joints. The thermal resistance of the solder joint in the FCLED package indicated a similar tendency in the temperature profiles of the FCLED package. The FCLED package bonded with Sn58Bi/0.1Ag-MWCNTs showed a lower total thermal resistance compared to that of the Sn58Bi solder joints, as observed in the measurements for the operating temperature and thermal conductivity. Heat generated from the FCLED chip needs to be dissipated into the atmosphere or conducted into the Al heat sink in a metal PCB. The Ag-MWCNTs in the solder improved the thermal management of the FCLED package, as observed in the higher thermal conductivity of the MWCNTs shown in Fig. 9. However, the FCLED package with Sn58Bi/0.3Ag-MWCNT shows a higher operating temperature and thermal resistance than the FCLED package with the pure Sn58Bi solder joints even though Sn58Bi/0.3Ag-MWCNTs show a higher thermal conductivity. It was thought that the structural effects made the difference in the FCLED package results. The agglomeration of the MWCNTs formed voids in the solder joints and hindered heat dissipation. Thus, the addition of Ag-MWCNTs indeed improves the thermal conductivity of the Sn58Bi solder and is an effective method to improve the thermal management of the FCLED package if the amount is not excessive.

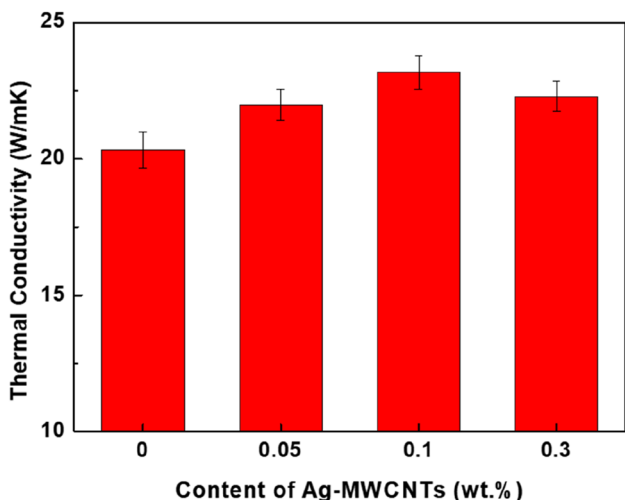


Fig. 9 Thermal conductivity of Sn58Bi with 0.3 wt% Ag-MWCNTs

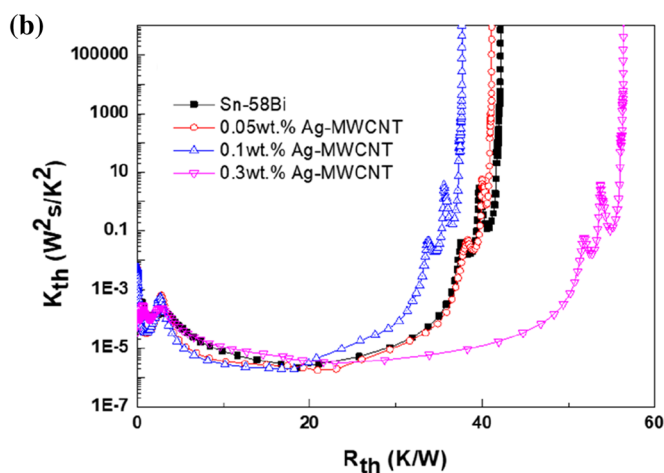
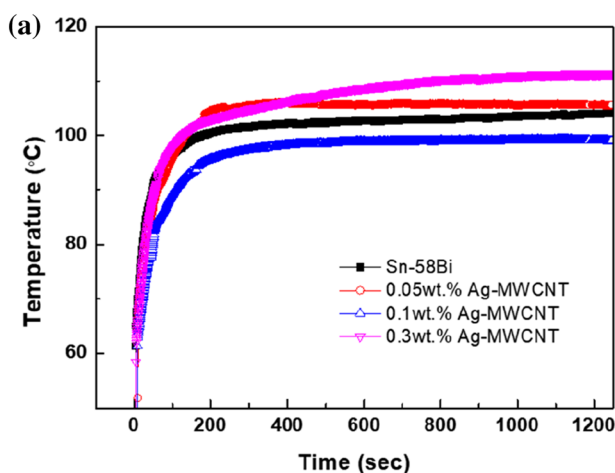


Fig. 10 a Temperature profiles of the FCLED package, and b Thermal resistance variations of solder joints with the addition of Ag-MWCNTs

## 4 Conclusion

We investigated the effect of the addition of Ag-MWCNTs on the thermal, mechanical, and electrical properties of solder joints in an FCLED package. The chemical composition of the IMC layers at the interfaces between the solder and the pad did not change. However, the IMC thicknesses of the solder joints decreased with the addition of Ag-MWCNTs. The Ag-MWCNTs in the solder joints retarded the growth of the IMC layers, and the shear strength and fracture energy of the solder joints with 0.05 wt% of Ag-MWCNTs improved by 16% and 80%, respectively, compared to those of the pure Sn58Bi solder. The electrical resistance of the solder alloys decreased as the Ag-MWCNT contents increased due to the electrical path by the net structure of the Ag-MWCNTs in the solder matrix. Also, the thermal resistance of the Sn58Bi solder with 0.1 wt% of Ag-MWCNTs decreased by a factor of 2. However, the FCLED package with 0.3 wt% of Ag-MWCNT shows a higher thermal resistance than the other FCLED packages, indicating that the agglomeration of the MWCNTs hindered heat dissipation.

**Acknowledgments** This research was supported by the Basic Science Research Program through the National Research Foundation of Korea (NRF), funded by the Ministry of Education (No. 2019R1A6A1A03033215). This material is based upon work supported by the Ministry of Trade, Industry & Energy (MOTIE, Korea) under the Industrial Technology Innovation Program. No. 20006956, 'Development of underfill material and package module with high thermal-shock ( $\geq 2000$  cycles) and mechanical drop reliability for mobile applications.'

## References

- S.M.L. Nai, J. Wei, M. Gupta, J. Electron. Mat. **37**, 515 (2008)
- S. Chantaramanee, S. Wisutmethangoon, S. Sikong, T. Plookhphol, J. Mater. Sci. Mater. Electron. **24**, 3707 (2013)
- X. Hu, Y. Li, Z. Min, J. Mater. Sci. Mater. Electron. **24**, 2027 (2013)
- M.S. Suh, C.J. Park, H.S. Kwon, Mater. Chem. Phys. **110**, 95 (2008)
- L.T. Chen, C.M. Chen, J. Mater. Res. **21**, 962 (2006)
- X. Hu, X. Yu, Y. Li, Q. Huang, Y. Liu, Z. Min, J. Mater. Sci. Mater. Electron. **25**, 57 (2014)
- H.W. Miao, J.G. Duh, B.S. Chiou, J. Mater. Sci. Mater. Electron. **11**, 609 (2000)
- F. Hua, Z. Mei, J. Glazer, in *IEEE Electron. Compon. Technol. Conf.* (1998), p. 277
- Z. Mei, F. Hua, J. Glazer, in *IEEE/CPMT International Electronics Manufacturing Technology Symposium* (1997), p. 463
- Y.D. Tsai, C.C. Hu, C.C. Lin, Electrochim. Acta **53**, 2040 (2007)
- C.Z. Liu, W. Zhang, J. Mater. Sci. **44**, 149 (2009)
- M. McCormack, H.S. Chen, G.W. Kammlott, S. Jin, J. Electron. Mater. **26**, 954 (1997)
- C. Fuchs, T. Schreck, M. Kaloudis, J. Mater. Sci. **47**, 4036 (2012)
- S.T. Oh, J.H. Lee, Electron. Mater. Lett. **10**, 473 (2014)
- W.R. Myung, M.K. Ko, Y. Kim, S.B. Jung, J. Mater. Sci. Mater. Electron. **26**, 8707 (2015)
- W.R. Myung, Y. Kim, S.B. Jung, J. Alloy. Compd. **615**, S411 (2014)
- J. Kim, W.R. Myung, S.B. Jung, Microelectron. Packag. Soc. **21**, 1 (2014)
- W.R. Myung, Y. Kim, K.Y. Kim, S.B. Jung, J. Electron. Mater. **45**, 3651 (2016)
- K.M. Kumar, V. Kripesh, A.A.O. Tay, J. Alloy. Compd. **455**, 148 (2008)
- L. Yang, W. Zhou, Y. Liang, W. Cui, P. Wu, Mater. Sci. Eng. A **642**, 7 (2015)
- J.P. Salvétat-Delmotte, A. Rubio, Carbon **40**, 1729 (2002)
- P. Sudan, A. Züttel, Ph Mauron, Ch Emmenegger, P. Wenger, L. Schlapbach, Carbon **41**, 2377 (2003)
- H.R. Kotadia, A. Panneerselvam, M.A. green, S.H. Mannan, in *12th IEEE international conference on Nanotechnology (IEEE-NANO)* (2012), p. 1
- H. Sun, Y.C. Chan, F. Wu, Mater. Sci. Eng. A **656**, 249 (2016)
- Y. Feng, H. Yuan, J. Mater. Sci. **39**, 3241 (2004)
- B. Zhao, B.L. Yadian, Z.J. Li, P. Liu, Y.F. Zhang, Surf. Eng. **25**, 31 (2009)
- D.J. Chakrabarti, D.E. Laughlin, Bull. Alloy Phase Diagr. **5**, 148 (1984)
- Z. Mei, J.W. Morris Jr., J. Electron. Mater. **21**, 599 (1992)
- L. Bokobza, J. Zhang, Polym. Lett. **6**, 601 (2012)
- A. Allaoui, S. Bai, H.M. Cheng, J.B. Bai, Compos. Sci. Technol. **62**, 1993 (2002)
- Y.D. Han, H.Y. Jing, S.M.L. Nai, L.Y. Xu, C.M. Tan, J. Wei, J. Electron. Mater. **41**, 2478 (2012)
- S.M.L. Nai, J. Wei, M. Gupta, J. Alloys Compd. **473**, 100 (2009)
- C.R. Barrett, W.D. Nix, A.S. Tetelman, *The Principles of Engineering Materials* (Prentice-Hall, Englewood Cliffs, NJ, 1973), p. 386
- O.S. Es-said, H.D. Merchant, J. Less-Common Met. **102**, 155 (1984)

**Publisher's Note** Springer Nature remains neutral with regard to jurisdictional claims in published maps and institutional affiliations.